Modeling Planarization in Chemical-Mechanical Polishing

Leonard Borucki[*],
Dilek Alagoz[†], Stephanie Hoogendoorn[‡],
Satyanarayana Kakollu[§], Maria Reznikoff[¶],
Richard Schugart[‖], and Michael Sostarecz[**]

June 24, 2002

Abstract

A mathematical model for chemical-mechanical polishing is developed. The effects of pad bending, fluid flow, and friction are considered. Fluid flow and friction effects are determined to be insignificant in the current model. Numerical results for the model including pad bending are presented and compared to experimental data.

1 Problem Description

1.1 Physical Problem

Chemical-mechanical polishing (CMP) is a process that is used to remove surface irregularities and to obtain uniform planarization of a silicon wafer surface. One application in which planarization is essential is the manufacture of computer chips.

During planarization, a wafer held upside down by a rotating wafer carrier is pressed against a rotating polishing pad as illustrated in Figure 1. Additionally, a chemically-reactive slurry containing fine abrasive particles is applied to the rotating pad. The chemicals in the slurry soften a thin layer of the wafer. The

[*]Motorola
[†]University of Kentucky
[‡]University of Pittsburgh
[§]Mississippi State University
[¶]Courant Institute of Mathematical Sciences
[‖]North Carolina State University
[**]Pennsylvania State University

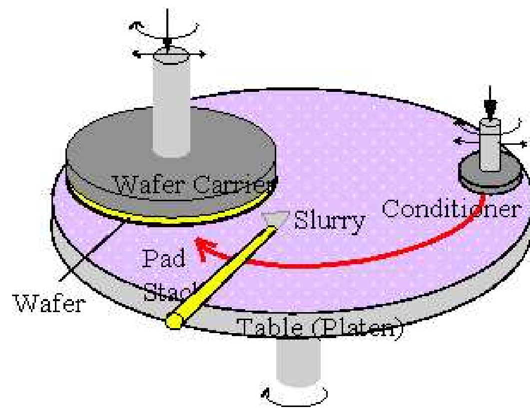

Figure 1: Chemical-Mechanical polishing tool

pad surface is covered with a large number of voids and bumps or asperities, as shown in Figure 2. When a load is applied to the wafer, the distance between the mean surface of the pad and the wafer decreases. Those asperities which are tall enough to reach the wafer surface drag the slurry particles across the surface. The combined mechanical and chemical actions are believed to be responsible for the polishing.

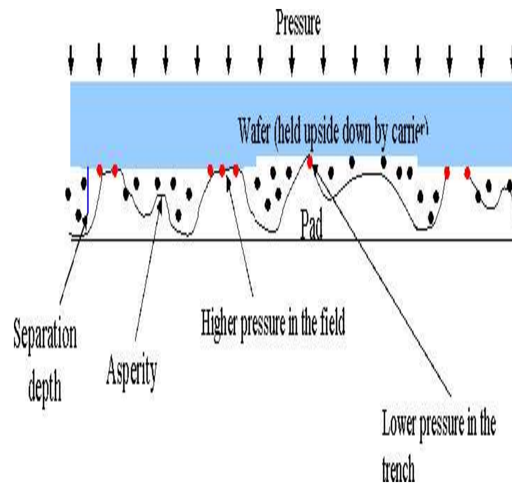

Figure 2: Detailed view of the wafer, trench, and pad

1.2 Experimental Observations

Laboratory experiments have been conducted to study how much material is removed from the wafer. To simulate observed surface irregularities, isolated rectangular trenches with varying depths and widths are etched onto a silicon wafer. The amount of removed wafer material is measured in both the trench and field (non-trench) areas. Less material is removed from the trenches than from the field. As indicated in Figure 2, the contact pressure is lower in the trenches than in the field. Developing a mathematical model that relates the pressure to the removal rate would be useful in coming to understand and refine the CMP process.

The problem is to model the CMP process and match the following given experimental results comparing the amount of material removed as a function of trench width and depth, as shown in Figure 3.

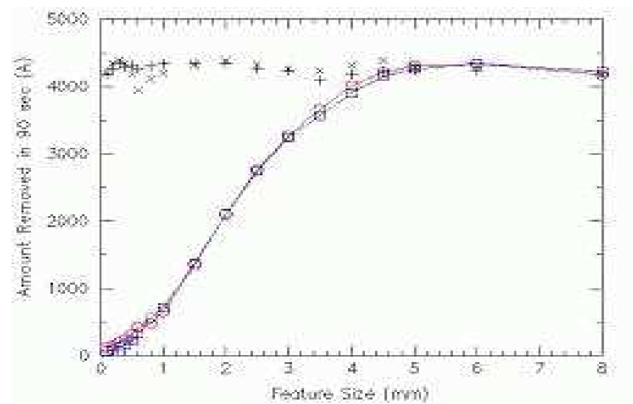

Figure 3: Experimental data of interest

In particular, the following questions summarize the interesting features of this data and will be considered:

1. Why does the removal rate at a trench bottom decrease exponentially with depth for small trench widths?
2. Why is the slope (on a log plot) of the amount removed at the trench bottom vs. depth nearly independent of the width for small trench widths?
3. The bottom removal curves in Figure 3 all appear to have a maximum at around 6 mm. Is this real?
4. The data ends at 0.1 mm, yet most trenches in real circuits have widths in the 0.1 to 10 μm range. What would be expected to happen for such narrow trenches?

2 Basic Model

The main goal is to develop a mathematical model of chemical-mechanical polishing of a wafer with an isolated trench. A successful model will capture the relationships between removal amount and trench width and depth that were observed experimentally. The heart of the model is the force balance equation:

$$L_{total} = L_{trench} + L_{field}$$
$$P_{total}A_{total} = P_{trench}A_{trench} + P_{field}A_{field},$$

where L is load, P is pressure, and A is area. Dividing by total area, we derive the pressure equation

$$P_{total} = \alpha P_{trench} + (1-\alpha)P_{field}, \quad (1)$$

where α is the area fraction A_{trench}/A_{total}.

To develop useful expressions for the trench and field pressures, the Greenwood-Williamson model is used. After having solved for the nominal trench and field pressures, Preston's Law is applied to calculate the amount removed. These two pieces of theory are discussed in the following subsections.

2.1 Greenwood-Williamson Model

The Greenwood-Williamson model can be used to relate nominal contact pressure to the separation distance between the wafer and the pad mean surface. It builds on Hertzian contact theory, in which the load on a sphere is related to the displacement of the sphere center via

$$L = \frac{4E}{3(1-\nu^2)\kappa^{1/2}}\delta^{3/2},$$

where L is load, E is Young's modulus, ν is the Poisson ration, κ is curvature, and δ is displacement. In applying the theory to CMP, we model the asperities as elastic spheres of constant curvature. Clearly, this is an idealization.

The height of the asperities above the pad mean surface is given by a probability density function, $\phi(z)$ (available as experimental data). Let N_{field} be the total number of asperities in the field. Then the number of asperities of height between z and $z+\Delta z$ is approximately $N_{field}\phi(z)\Delta z$. Also, if d is the "separation distance" between the wafer and the pad mean surface, then the displacement δ of an asperity of height $z > d$ is $z - d$. The total load in the field area is then given as the sum of the load of all asperities in the field of height greater than or equal to d, which

is calculated as the integral

$$
\begin{aligned}
L &= \int_d^\infty L_{asperity} N_{field} \phi(z) dz \\
&= \frac{4E}{3(1-\nu^2)\kappa^{1/2}} N_{field} \int_d^\infty (z-d)^{3/2} \phi(z) dz.
\end{aligned}
$$

Dividing by field area to get pressure, we replace N_{field}/A_{field} by the asperity density, η, to arrive at

$$
P_{field} = C \int_d^\infty (z-d)^{3/2} \phi(z) dz, \tag{2}
$$

where for ease of notation, we define $C \equiv \frac{4E\eta}{3(1-\nu^2)\kappa^{1/2}}$. Although there is uncertainty as to the exact value of η and E for the experiment at hand (note that the Young's modulus of a single asperity will differ from the Young's modulus of the bulk pad), we are able to solve for the constant C using experimental data (see Section 4.2).

In the trench, we need to modify the pressure expression slightly to account for the trench height. Assuming as a first approximation that the pad mean surface remains flat in the trench area, the expression for trench pressure can be seen to be

$$
P_{trench} = C \int_{d+h}^\infty (z-d-h)^{3/2} \phi(z) dz, \tag{3}
$$

where h is the trench height.

Substituting (2) and (3) into (1), we arrive at the following formula for pressure as a function of separation distance

$$
P_{total}(d) = C \left(\alpha \int_{d+h}^\infty (z-d-h)^{3/2} \phi(z) dz + (1-\alpha) \int_d^\infty (z-d)^{3/2} \phi(z) dz \right).
$$

The basic idea of the model is to invert the above formula to solve for separation distance, given the applied load. Substituting d back into (2) and (3), we obtain the field and trench pressure, respectively. To transform pressure information into removal rate, we turn to Preston's Law.

2.2 Preston's Law

Differences in contact pressure have been shown to lead to surface height reductions. Experimentally, the removal rate can be described by Preston's law

$$
\frac{\Delta \text{height}}{\Delta \text{t}} \propto vP \tag{4}
$$

where v is the relative sliding velocity and P is the nominal contact pressure. The constant of proportionality can either be determined from experimental data or by the approximation $\frac{1}{2E}$. Thus, using the pressure information with Preston's law, the removal rate can be calculated.

3 Modeling Physical Behavior

There are a multitude of physical factors which play a role in the CMP process. The present work considers three of these factors: pad bending, fluid pressure, and friction, and analyzes whether incorporating them into the "basic model" would be significant.

3.1 Pad Bending

As a first approximation in the basic model, we assume that the pad mean surface remains flat in the trench area. In fact, as the wafer presses down on the polishing pad, the pad (which has a Young's modulus $E \approx 540e6Pa$ and Poisson ratio $\nu \approx 0.45$ compared to the wafer of $E \approx 112.4e9Pa$ and $\nu \approx 0.28$) will deform, with the mean surface undergoing a positive vertical displacement. We call this physical behavior pad bending, as illustrated in Figure 4

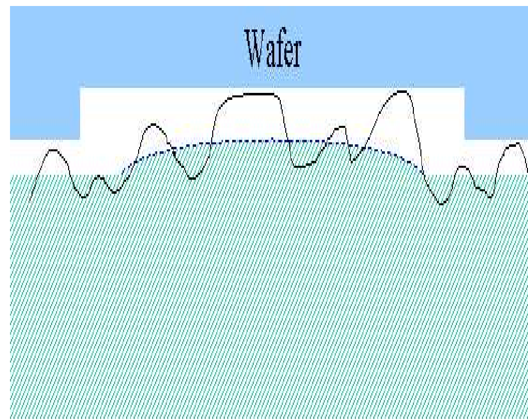

Figure 4: Pad bending

It seems clear that pad bending will be a significant factor in the trench pressure calculation. Without bending, mechanical contact between asperities and the trench bottom will be a rare event. With bending, however, shorter asperities will be able to make contact with the trench bottom, increasing predicted pressure and polishing in the trench.

The remainder of this section is concerned only with the portion of the pad in the trench area, since that is where pad bending occurs. Also, in modeling the mechanical behavior of the pad, it was appropriate to consider the CMP set-up in more detail than discussed in the previous sections. Specifically, the polishing pad ("hardpad") is a $1.3mm$ thick pad that rests on a second, "softpad", also $1.3mm$ thick, which is glued to the platen. The material properties of the hard and soft pad are given at the end of the subsection.

Pad bending will enter into the model by modifying the limit and integrand in equation (3). There are different ways in which inclusion of the vertical displacement profile can be implemented. Two possible modifications of (3) are

$$P_{trench} = C \int_{d+h-b^*}^{\infty} (z - d - h + b^*)^{3/2} \phi(z) dz \tag{5}$$

$$P_{trench} = C \frac{1}{w_T} \int_0^{w_T} \int_{d+h}^{\infty} (z - d - h)^{3/2} \phi(z) dz dx, \tag{6}$$

where w_t is the width of the trench. In (5), a special value for the displacement, b^*, is chosen, which might be the average displacement or the displacement at the center of the trench, for example. In (6) a different approach is taken, substituting the pointwise value for displacement as a function of x and averaging over the width of the trench afterwards. In the model, we will use (5) with b^* the displacement at the center of the trench, since that is where the experimental measurements were made. We now consider solving for the displacement.

One way to model pad bending is to treat the pad surface as an elastic beam. Although this method is rejected in what follows, it is included here for completeness and because it provides an opportunity to mention two interesting ideas that arise in consideration of the beam model.

The equation for the displacement, $b(x)$ of a thin beam is

$$EI \frac{d^4 b}{dx^4} = P, \tag{7}$$

where I is the moment of inertia and P is the load per unit length, and we take as our domain $0 < x < w_T$. For the model problem with no trench contact, P is a constant and the solution to (7) is easily seen to be

$$b(x) = \frac{1}{EI} \left(P \frac{x^4}{24} + c_1 \frac{x^3}{6} + c_2 \frac{x^2}{2} + c_3 x + c_4 \right),$$

where the constants c_i are determined from the boundary conditions.

Two ideas which arise in consideration of the beam model are the following. First, while raising the pad mean surface, bend reduces the vertical height of an individual asperity above the mean surface by tilting it. If it is assumed that the tip of the asperity remains the highest point after tilting, then the height z of an asperity above the mean surface will transform to $\frac{z}{\sqrt{1+b'(x)^2}}$. This idea is mentioned here because it is particularly easy to imagine implementing the correction factor with the beam formulation, although of course it could be included in any pad bending implementation where $b'(x)$ is either known or can be well approximated. The correction factor is not included in the current model, and whether or not it would have a noticeable effect on the quantitative output is not known.

The second issue which quickly arises in considering the beam model is the effect of trench-bottom-contact. Once the trench asperities make contact with the wafer, they absorb some of the load and the right hand side of (7) becomes

considerably more complicated. The new equation to solve is

$$EI\frac{d^4b}{dx^4} = P - C\int_{d+h-b(x)}^{\infty}(z-d-h+b(x))^{3/2}\phi(z)dz.$$

One approach to solving the above equation would be to use (7) to get a first approximation for $b(x)$ to use in the rhs, and iterate the process to find b. Again, trench-bottom-contact could be included in other more appropriate analytical models of pad bending, but that work has not been done at this time.

The main reason for rejecting the beam model is that treating the pad surface as a thin beam is conceptually inappropriate. The hard pad itself is not thin ($1.3mm$) compared to the trench width ($\sim 0.1 - 6.0mm$), and the pad surface cannot move independently of the rest of the pad. A more appropriate analytical model to use might be that of an elastic half-space, at least for small trench widths.

In place of the beam model, numerical simulations using FEMLAB are used to calculate the mean surface displacement. Using the plane strain module, the experimental set-up is modeled as a section of wafer, a section of hardpad, and a section of softpad. The trench width is allowed to vary from $0.1mm$ to $2.0mm$. On either side of the trench, $4.4mm$ of wafer are included, which should be a broad enough section to give good results for trench-area-displacement. The height, Young's modulus, and Poisson ratio of the wafer, hardpad, and softpad are: 0.5 mm, 112.4 e9 Pa, 0.28; 1.3 mm, 540 e6 Pa, 0.45; and 1.3 mm, 2.7 e6 Pa, 0.1, respectively. Zero-displacement boundary conditions are enforced on the bottom edge, while a pressure of -2.8 e4 Pa is applied to the top edge of the stack. FEMLAB solves the plane strain elasticity problem, and the vertical displacement of the pad surface at the trench center is recorded for use in the model, as previously discussed.

FEMLAB predicts trench center displacement to be linear in trench widths for small widths (of the order of $0.1 - 0.8mm$), in accordance with experimental observation. The FEMLAB results highlight the fact that flat surface theory over-predicts the width at which mechanical polishing begins. Experimental data demonstrating that mechanical polishing takes place at trench widths too narrow for the bulk pad to have reached the trench bottom make it clear that it is important to consider the role of the pad asperities. Note that the pad bending will actually be greater than the current results indicate, because of the decreased effective Young's modulus of the asperity layer (see the end of Section 3.3). A better approximation of the pad bending could be performed by including a narrow asperity layer in the FEMLAB simulations. A more detailed consideration of the role of the asperity layer geometry in pad bending would be interesting and difficult. Finally, it may be worthwhile to remark that FEMLAB can also be considered a tool with which to explore the appropriate boundary conditions for an analytical model of pad bending. While it is clear that $b(0) = b(w_T) = 0$, the derivative condition is less obvious. An initial guess for the correct boundary conditions was the clamped condition, $b'(0) = b'(w_T) = 0$. The FEMLAB calculations yield ~ 0.003 for the initial and final slope.

3.2 Fluid Pressure

Since there is slurry fluid between the pad and the wafer, there is an additional fluid pressure within the trench that should be modeled. In order to calculate the fluid pressure, we need to consider the Navier Stokes equations for Newtonian, incompressible fluid flow

$$\frac{\partial \mathbf{u}}{\partial t} + \mathbf{u} \cdot \nabla \mathbf{u} = -\frac{\nabla p}{\rho} + \frac{\mu}{\rho} \nabla^2 \mathbf{u} \tag{8}$$

$$\nabla \cdot \mathbf{u} = 0 \tag{9}$$

where $\mathbf{u} = (x, y, z, t)$ is the fluid flow (or velocity), $p(x, y, z, t)$ is the pressure, ρ is the fluid density, and μ is the (dynamic) viscosity. Equation 8 expresses the fluid's conservation of mass and momentum, while Equation 9 is the incompressibility condition of the fluid.

We solve the Navier Stokes equations by considering the physical characteristics of the wafer. Since the fluid is a steady flow within a two-dimensional cross section of the trench, we set $\frac{\partial \mathbf{u}}{\partial t} = 0$, and the flow takes the form $\mathbf{u} = (u(x, z), 0, w(x, z))$. Further, the flow is contained between two rigid boundaries given by $z = 0$ and $z = h(x)$.

When the Navier Stokes equations are non-dimensionalized (that is, the orders of magnitude of the Navier Stokes terms are compared), Equations 8 and 9 can be written in a solvable form; this is quite a remarkable circumstance (see Reference [1], §7.6). In the model, the scale of the length of the wafer (mm) is much greater than that of the fluid height (μm) (where these dimensions correspond to the x and z scale, respectively). This fact produces two significant results. First due to both properties of the incompressible flow and that $x >> z$, the magnitude of the viscous term ($\nabla^2 \mathbf{u}$) dominates the magnitude of the non-linear convection term ($\mathbf{u} \cdot \nabla \mathbf{u}$). Hence it is not necessary to consider the non-linearity and the resulting non-dimensionalized system *greatly* reduces to

$$\begin{aligned} p_x &= \mu \, u_{zz} \\ p_z &= \mu \, w_{zz}. \end{aligned}$$

Secondly, because the vertical component of the fluid velocity, w, is much smaller than the horizontal velocity, the pressure, to a first approximation, is constant in the vertical direction, so that $p_z = 0$ Thus $p_x = \mu \, u_{zz}$ can be integrated with respect to z, so that the fluid flow can be expressed as

$$u(x, z) = \frac{1}{2\mu} P_x z^2 + k_1(x) z + k_2(x). \tag{10}$$

The next step is to obtain an expression for the fluid pressure. Since F $=$ m $\cdot$ a, the flux across a rectangular cross section taken at an arbitrary x inside the trench is

$$\int_0^{h(x)} m \; u_x(x, z) \; dz$$

where $z = h(x)$ is the fluid film thickness and $m = \frac{\rho}{\text{volume}}$. Since the fluid is incompressible, apply conservation of mass (the flux entering equals the flux leaving), to obtain

$$\int_0^{h(x_1)} m\ u_x(x_1, z)\ dz = \int_0^{h(x_2)} m\ u_x(x_2, z)\ dz$$

which simplifies to

$$\frac{d}{dx} \int_0^{h(x)} u(x, z) dz = 0. \tag{11}$$

Substituting Equation 10 into Equation 11, we obtain the following form of the Reynolds equation that relates the fluid film thickness, $h(x)$, to the fluid pressure

$$\frac{d}{dx}\left(\frac{h^3}{6\mu}\frac{dp(x)}{dx}\right) = -\left(k_1(x)h + k_2(x)\right)\frac{dh}{dx} - \left(k_1^{'}(x)\frac{h^2}{2} + k_2^{'}(x)h\right).$$

Because of the dependence of fluid flow on friction, a discussion of the role of fluid flow is deferred until the end of the next subsection.

3.3 Wafer Tilt Angle Calculation

A frictional force opposite to the velocity direction causes the wafer to tilt with tilt angle α between the wafer and the mean surface pad. This tilt angle produces a non-uniform fluid flow within the trench that effects the fluid pressure, as shown in Figure 5.

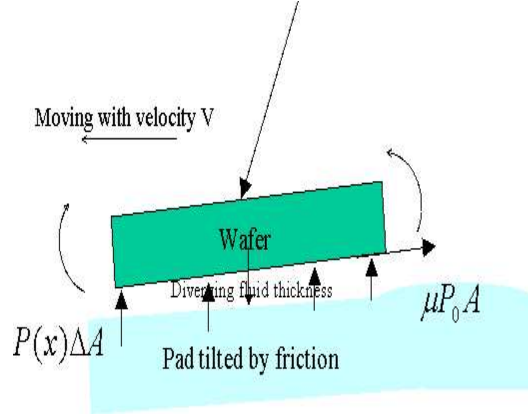

Figure 5: Angle tilt due to friction

Considering the effects of friction along the surface of the wafer, friction will cause the wafer to tilt. Assuming a linear fluid pressure along the wafer, a linear equation from elasticity theory for pressure across the wafer is

$$P(x) = \frac{M}{h_p}\left(\delta - R + \tan\alpha x\right) = \frac{M}{h_p}\left(\delta - R + \alpha x\right), \tag{12}$$

where h_p is the height of the pad, R is the radius of the wafer, α is the wafer tilt angle, E is Young's modulus, ν is the Poisson ratio, δ is the displacement, and $M = \frac{E\nu}{(1+\nu)(1-2\nu)}$. Assume that α is small and approximate $\tan\alpha \approx \alpha$. To simplify the calculations, converting Equation 12 to polar coordinates, we obtain

$$P(r,\theta) = \frac{M}{h_p}(\delta - R + \alpha r\cos\theta).$$

Using $P(r,\theta)$ in a force balance, the equation

$$\int_0^{2\pi}\int_0^R P(r,\theta) r \mathrm{d}r\mathrm{d}\theta = P_0\pi R^2 \tag{13}$$

is obtained where P_0 is the average applied nominal contact pressure. Using $P(r,\theta)$ in a moment balance, the equation

$$\begin{aligned} m_w g\frac{h_w}{2}\sin\alpha - \mu h_w \int_0^{2\pi}\int_0^R P(r,\theta) r\mathrm{d}r\mathrm{d}\theta &= m_w g\frac{h_w}{2}\alpha - \mu h_w \int_0^{2\pi}\int_0^R P(r,\theta) r\mathrm{d}r\mathrm{d}\theta \\ &= \int_0^{2\pi}\int_0^R P(r,\theta) r^2\cos\theta\mathrm{d}r\mathrm{d}\theta, \end{aligned} \tag{14}$$

is obtained where m_w is the mass of the wafer, g is the acceleration due to gravity, h_w is the height of the wafer, and μ is the coefficient of friction. Again, assuming that α is small, $\sin\alpha \approx \alpha$. Substituting the results from the force balance (Equation 13) into the moment balance (Equation 14) and then solving for α we have,

$$\alpha = \frac{\mu P_0 \pi R^2 h_w}{\frac{m_w g h_w}{2} - \frac{M\pi R^4}{4h_p}}.$$

Since $E = 540 * 10^6$ Pa, $\nu = 0.45$, $\mu = 0.4$, $P_0 = 28000$ Pa, $R = 100$ mm, $h_w = 0.5$ mm, $m_w = 8.85$ g, $g = 9.8\ \frac{\mathrm{m}}{\mathrm{s}^2}$, and $h_p = 1.3$ mm, the tilt angle is calculated to be $\alpha = -1.7476 * 10^{-8}$.

To improve this calculation, an effective Young's modulus can be calculated. The Young's modulus of the pad is a bulk property. However, the part of the pad with which the wafer is in contact is the rough pad surface, and the asperities provide significantly less surface area contact than would an ideally flat pad. As a result, the wafer "feels" a different, effective Young's modulus. To take this into account, an effective Young's modulus was calculated for the wafer in contact with the asperities by linearizing the pressure around P_0, the average applied nominal contact pressure. This calculation yields a tilt angle of $\alpha = -3.1975 * 10^{-7}$.

Remark 3.1. For both the fluid pressure and the tilt angle, we determined that the numerical effects of including these behaviors in the model are insignificant, and thus the final version of the model neglects these two physical behaviors. We believe that both these behaviors, perhaps in combination with additional factors, should probably be included in a full model of the CMP process.

4 Numerical Approximations

The two remaining details that are needed in order to complete the calculations are the Pearson distribution and the expression of experimental constants, C. These will be now be discussed.

4.1 Pearson Distribution

The pad surface height probability distribution function is often not Gaussian but can usually be described by one of the Pearson family of distributions, which are solutions of

$$\frac{\mathrm{d}\phi}{\mathrm{d}z} = \frac{a - z}{b_0 + b_1 z + b_2 z^2}\phi \tag{15}$$

for suitable values of a, b_0, b_1, and b_2. Solving the differential equation,

$$\phi(z) = k\left(b_0 + b_1 z + b_2 z^2\right)^{-\frac{1}{2b_2}} \mathrm{e}^{\frac{b_1 + 2ab_2 \tan^{-1}\left(\frac{b_1 + 2b_2 z}{\sqrt{4b_0 b_2 - b_1^2}}\right)}{b_2\sqrt{4b_0 b_2 - b_1^2}}} \tag{16}$$

is obtained where k is the constant of integration. Note that sometimes the probability distribution function can be approximated by a Gaussian if b_1 and b_2 are small. If $b_1 = b_2 = 0$ in the above differential equation, then this is the differential equation for the Gaussian distribution.

To find the values of the five constants a, b_0, b_1, b_2, and k, a least-squares minimization was done by using the Matlab function *fminsearch* with a set of height probability distribution data. The function *fminsearch* requires an initial guess of the five constants to find a local minimum in a five-dimensional parameter space. A reasonable initial guess was obtained by using some statistical theory, Mathematica, and the assumption that $k = 1$. Using the calculated initial guess with *fminsearch* yields

$$\begin{array}{rclrclrcl} a & = & 1.81151019 & b_0 & = & 55.68591263 & b_1 & = & -1.77381050 \\ b_2 & = & 0.11193788 & k & = & 1176103.6968 & & & \end{array}$$

with an error on the order of 10^{-6}. The units of $\phi(z)$ are nm^{-1}.

4.2 Calibrating Experimental Constants

To estimate the expression of experimental constants

$$C = \frac{4E\eta}{3(1-\nu^2)\kappa^{1/2}},$$

we used asperity height data from an independent CMP experiment. In the experiment, a conditioner was not used which implies that the asperities on the pad were left to be worn away during the polishing procedure. After polishing for 31 minutes without using the conditioner, the resulting probability density distribution on the pad was measured, as shown in Figure 6.

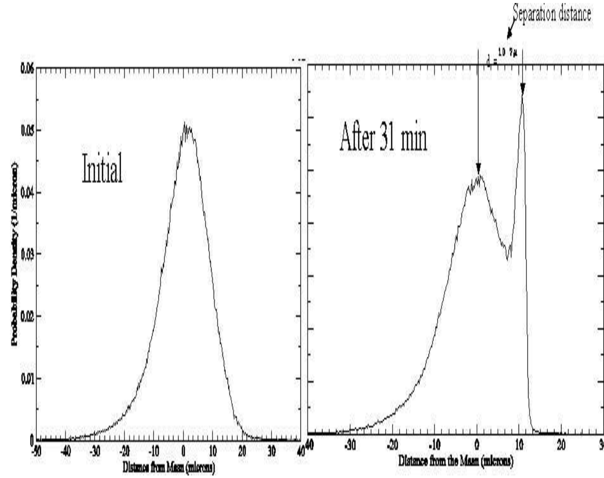

Figure 6: Probability density distributions before and after polishing without a conditioner

After polishing, the resulting distribution for asperity height shows a second peak. The asperities which were taller than the separation distance wore out during polishing until they no were no longer taller than the separation distance. This second peak corresponds to the separation distance. Substituting $d = 10.7\mu m$ and the known applied load into Equation 2, it is easy to calculate the following estimate for C

$$C = \frac{P}{\int_d^\infty (z-d)^{3/2}\phi(z)dz}.$$

This value for C was used in the model.

5 Numerical Results

Using Matlab, we ran our code for 10 trench heights ranging from .2 to 2 μm, 12 trench widths ranging from .1 to 2 mm, and two probability density functions for our asperity heights. The first was taken from experimental data. Since this data was not taken from the same pad that was used for our polishing data, we also used a Gaussian distribution that was comparable but had a lower standard deviation. We also had planned to use a Pearson Distribution, but ran into time constraints. In our model, the only effect from trench width comes from pad bending. Neglecting this for the moment, our results, shown in Figure 7, using the sample PDF clearly shows an exponential decay of trench wear as trench height is increased as is also noticed in the polishing data. Our numerics also show a field wear of $.46\mu m$ in 90 seconds which was comparable to the data which had field wear between .41 and .43 μm. Also, our model showed trench wear approaching field wear as trench height is decreased as would be expected. Unfortunately,

our decay rate was much less than that compared with the experimental data. When we switched to the Gaussian PDF, as shown in Figure 8, our decay rate was improved, but still did not match experimental data.

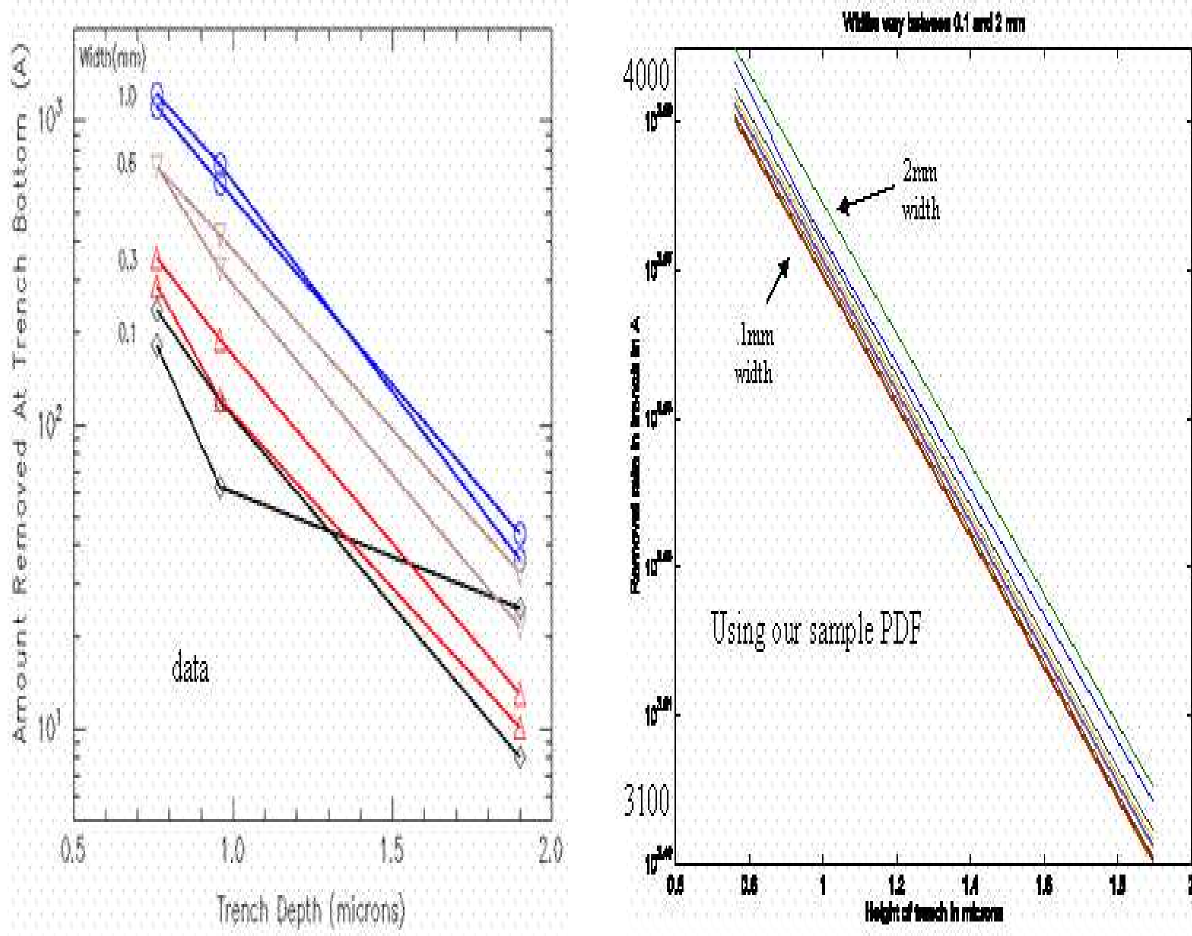

Figure 7: Experimental data compared to numerical results which use experimental PDF data

Taking into account pad bending, we used our results from FEMLAB that measured how the pad below the center of the trench was raised as the trench width was increased. For our smallest trench widths (.1 to .75 mm), the pad bending was linear, thus giving an effect of linearly reducing trench height. Thus for these trench widths, our model shows exponential growth of trench wear as trench width was increased which was qualitatively in agreement with experimental polishing data. However, for our larger trench widths (1 to 2 mm), the pad bending appeared quadratic, giving an affect of greater than exponential growth of trench wear as trench width was increased.

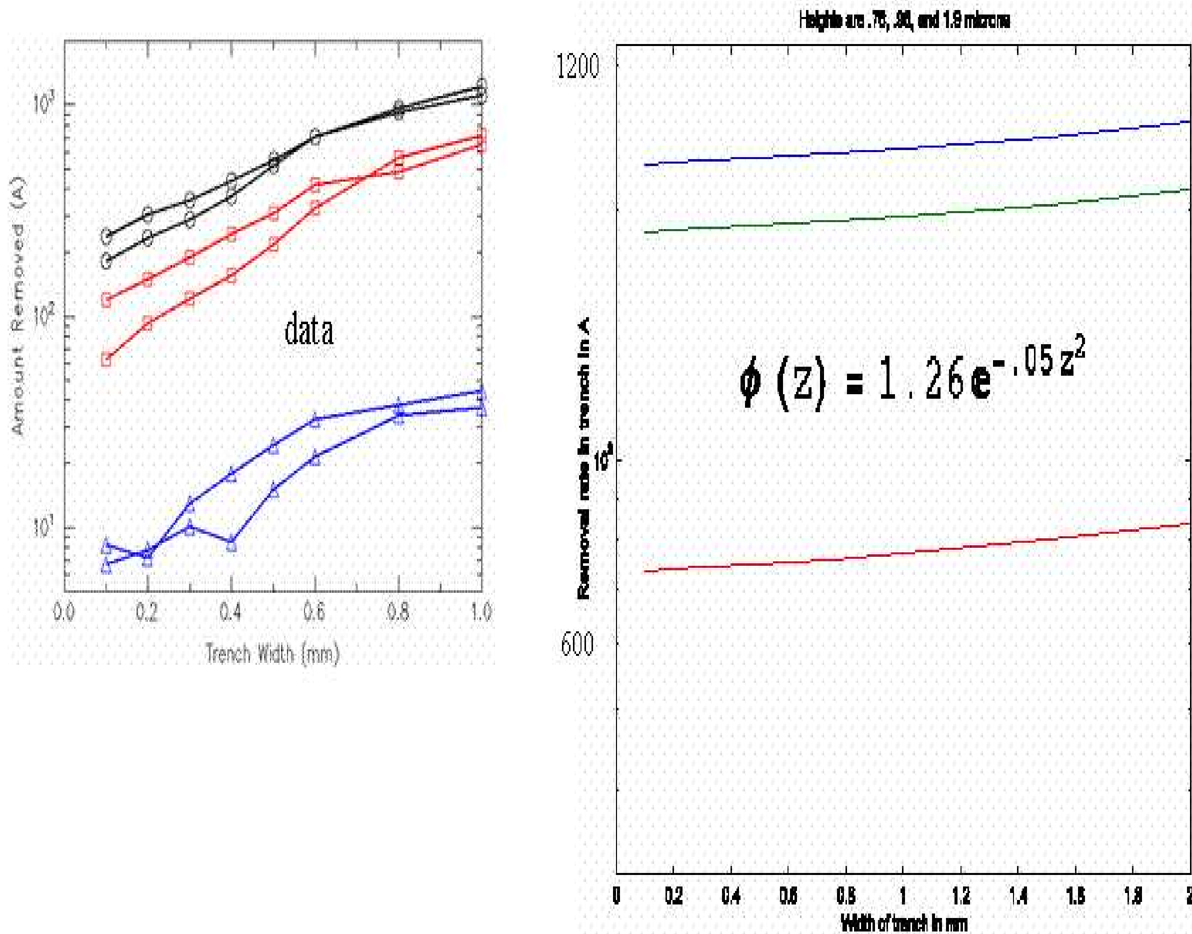

Figure 8: Experimental data compared to numerical results which use a Gaussian PDF

6 Conclusions

We conclude by summarizing our qualitative answers to the four questions listed in Section 1.2. When possible, these results are supported by output from our model. The model output is in qualitative agreement with the experimental evidence referred to in two of the questions, supporting the validity of the model.

1. Why does the removal rate at a trench bottom decrease exponentially with depth for small trench widths?

   Qualitatively, the idea is that this is the range in which pad bending becomes significant enough to allow substantial mechanical polishing to begin. If this is the dominant factor in the exponential growth, then our model, which focuses on the role of pressure and its relationship to trench depth and width (through bending), should reflect this behavior, as it does.

This is caused primarily by the distribution of the asperity heights. We fitted the given sample distribution to a Pearson Distribution, by using least square error as the criteria. This Pearson Distribution has an inverse tangent function of height as the argument for the exponential term. Interestingly the linear range of the tangent function lies in the region of interest, 0-15 μm. If a Gaussian were used to fit the distribution, we would have had a quadratic. However this only explains that the height distribution is exponential, but it would be reasonable to assume height is directly related to the material removed. Our model predicts this behavior.

2. Why is the slope (on a log plot) of the amount removed at the trench bottom vs. depth nearly independent of the width, for small widths $(0.1 - 1.0mm)$?

   Our model predicts this behavior, as shown in Figure 7

3. The bottom removal curves in Figure 3 all appear to have a maximum at around 6 μm. Is this real?

   The model doesn't predict this behavior. A hypothesis is that lateral deformation of the asperities is important. Once the trench is wide enough, the contact area of the pad in the trench is approximately equal to that in the field. The idea is that there may be a narrow width range in which the lateral asperity deformation actually renders polishing more effective in the trench, as with a brush with angled bristles.

4. The data ends at 0.1 mm, yet most trenches in real circuits have widths in the 0.1 to 10 μm range. What would be expected to happen for such narrow trenches?

   There will be a threshold width below which pad bending will not be great enough to allow significant asperity contact in the trench. At such widths, there will be very little mechanical polishing and, therefore, little material will be removed. It would be interesting, after getting more precise results for pad bending, to estimate the threshold width and compare to experimental data.

   For such narrow trenches we would expect that no material is removed from the bottom of the trenches, and a correction for the model would be introduced to indicate that at such small widths no material is removed from the trenches.

7 Future Work

While there are numerous, unexplored physical behaviors which contribute to the CMP, these topics directly follow from the results:

- Consider the effect of the aspect ratio of the trench on the slurry fluid flow
- Combine the fluid flow results with the convection-diffusion equation to determine depth of chemical action
- Further investigate the effects of the tilt angle

- Model the effects of the pad perforations
- Use the Pearson Distribution for the pad surface height probability distribution function
- Include a detailed geometric analysis of microscopic asperity behavior.

References

[1] D.J. Acheson, *Elementary Fluid Dynamics*, Okford University Press (1990).

[2] K.L. Johnson, *Contact Mechanics*, Cambridge University Press (1985).

[3] L.D Landau and E.M. Lifshitz, *Mechanics*, Pergamon Press (1976).

[4] J.A. Greenwood and J.B.P. Williamson, *Contact of Nominally Flat Surfaces*, Proceedings of the Royal Society of London, Series A, Mathematical and Physical Sciences, 295 (Dec. 6, 1966), pp. 300-319.

Acknowledgments

The students thank Len for his leading us through this insightful experience and for encouraging us to carry out simple experiments that build our intuition. We further acknowledge the use of his figures in this report.